# Gram-Negative Outer and Inner Membrane Models: Insertion of Cyclic Cationic Lipopeptides

**Adrià Clausell,[†] Maria Garcia-Subirats,[‡] Montserrat Pujol,[†] M. Antonia Busquets,[†] Francesc Rabanal,[‡] and Yolanda Cajal*,[†]**

*Physical Chemistry Department and Institute of Nanoscience and Nanotechnology, University of Barcelona, Av. Joan XXIII s/n, 08028 Barcelona, Spain, and Department of Organic Chemistry, University of Barcelona, Martí i Franquès 1, 08028 Barcelona, Spain*

*Received: July 26, 2006; In Final Form: October 18, 2006*

Most Gram-negative bacteria are susceptible to polymyxin B (PxB), and development of resistance to this cationic lipopeptide is very rare. PxB mechanism of action involves interaction with both the outer membrane (OM) and the inner membrane (IM) of bacteria. For the design of new antibiotics based on the structure of PxB and with improved therapeutic indexes, it is essential to establish the key features of PxB that are important for activity. We have used an approach based on mimicking the outer layers of the OM and the IM of Gram-negative bacteria using monolayers of lipopolysaccharide (LPS) or anionic 1-palmitoyl-2-oleoylglycero-*sn*-3-phosphoglycerol (POPG), respectively, and using a combination of penetration assay, analysis of pressure/area curves, and Brewster angle microscopy to monitor surface morphology changes. Synthetic analogue sp-B maintains the basic structural characteristics of the natural compound and interacts with the OM and the IM in a similar way. Analogue sp-C, with a mutation of the sequence [D-Phe$^6$-Leu$^7$] into [D-Phe$^6$-Dab$^7$], shows that this hydrophobic domain is involved in LPS binding. The significant role of the positive charges is demonstrated with sp-Dap analogue, where L-α,γ-diaminobutyric acid residues Dab$^1$ and Dab$^8$ are replaced by L-α,γ-diaminopropionic acid (Dap), resulting in lower degrees of insertion in both LPS and PG monolayers. The importance of the N-terminal acyl chain is demonstrated with polymyxin B nonapeptide (PxB-np). PxB-np shows lower affinity for LPS compared to PxB, sp-B, or sp-C, but it does not insert into PG monolayers, although it binds superficially to the anionic film. Since PxB microbial killing appears to be mediated by osmotic instability due to OM−IM phospholipid exchange, the ability of the different peptides to induce membrane−membrane lipid exchange has been studied by use of phospholipid unilamellar vesicles. Results indicate that cationic amphipathicity determines peptide activity.

## Introduction

The global emergence of multidrug-resistant bacteria is an important clinical problem that is increasingly limiting the use of currently known antibiotics. There is a great demand to find new drugs to overcome this problem, but experience has proven that the time to develop resistance to new antibiotics is often very short. This is essentially related to the mechanism of action of traditional antibiotics, with five main specific targets in the cell: cell-wall synthesis, DNA gyrase, metabolic enzymes, DNA-directed RNA polymerase, and protein synthesis.[1] Bacteria can develop genetic resistance toward these mechanisms of action at a rate that depends on many factors, such as the number of targets.

Antimicrobial peptides (AMPs) are a class of antibiotics that rarely spur the development of resistant microorganisms. AMPs are secreted by many living organisms in response to infection by Gram-negative and Gram-positive bacteria.[2−4] They are a diverse group of molecules, with more than 800 described so far.[5] Despite their diversity, the main target of most AMPs is the lipid bilayer itself, without any stereospecific interaction with chiral receptors or enzymes.[2,6] To develop genetic resistance is therefore very costly for the bacteria.

Polymyxin B (PxB) is a nonribosomally synthesized AMP produced by *Bacillus polymyxa*, with selectivity against Gram-negative bacteria, including multidrug-resistant *Acinetobacter baumannii* and *Pseudomonas aeruginosa* strains.[7−10] As do most AMPs, PxB has a highly amphipathic nature, an important feature for membrane interaction. A second important characteristic shared by most AMPs is a net cationic charge at physiological pH, with five positive charges due to L-α,γ-diaminobutyric acid (Dab) in the case of PxB. The cationic character of PxB facilitates its preferential interaction with the bacterial membranes, rich in anionic phospholipids such as phosphatidylglycerol and cardiolipin. In contrast, the outer leaflet of mammalian cell membranes mainly comprises phosphatidylcholine and cholesterol, which are charge-neutral at physiological pH. The mechanism of action of PxB involves the inner and outer membranes of the Gram-negative bacteria. PxB binds to the anionic surface molecule lipopolysaccharide (LPS) in the outer membrane (OM), leading to self-promoted uptake across the OM[11] and subsequently reaching the periplasmic space and interacting with the cytoplasmic membrane.[12] The mechanism of bacterial killing is clearly not related to membrane permeation, which takes place at concentrations well above the minimal inhibitory concentration (MIC).[7,11−13] The actual mech-

* Corresponding author: phone 34-93-4035988; fax 34-93-4035987; e-mail ycajal@ub.edu.
[†] Physical Chemistry Department and Institute of Nanoscience and Nanotechnology.
[‡] Department of Organic Chemistry.

10.1021/jp064757+ CCC: $37.00 
Published on Web 12/23/2006

**TABLE 1: Peptide Sequences**

| peptide | sequence[a] |
|---|---|
| PxB | $R_1$-Dab-Thr-Dab-*cyclo*[DabDab-D-Phe-Leu-DabDab-Thr] |
| PxB-np | Thr-Dab-*cyclo*[DabDab-D-Phe-Leu-DabDab-Thr] |
| sp-B | $R_2$-Dab-Thr-Dab-*cyclo*-[Cys-Dab-D-Phe-Leu-DabDab-Cys] |
| sp-C | $R_2$-Dab-Thr-Dab-*cyclo*-[Cys-Dab-D-Phe-Dab-Leu-Dab-Cys] |
| sp-D | $R_2$-Dap-Thr-Dab-*cyclo*-[Cys-Dab-D-Phe-Leu-Dap-Dab-Cys] |

[a] $R_1$, (*S*)-6-methyloctanoyl; $R_2$, nonanoyl; sp-B, sp-C, and sp-D are cyclized by means of a disulfide bond between Cys-4 and Cys-10.

anism of action is not yet fully understood but has been proposed to involve the formation of molecular contacts between the inner and outer membranes of the bacteria and the induction of lipid exchange, thus resulting in loss of the compositional specificity of the membranes and osmotic instability.[14−16] It is extremely difficult for the bacteria to generate genetic resistance to such a physical mechanism of action based on ionic and hydrophobic interactions. In fact, resistance to polymyxins is rare,[17,18] a reason that explains the renewed interest in the clinical use of PxB and related antibiotics.[8,9,18,19] In the search for new antibiotics with the same mechanism of action as PxB but with better therapeutic indexes, we have designed and synthesized a series of PxB-analogues (sequences are shown in Table 1 and molecular structures in Figure 1). Analogue sp-B maintains the basic features of PxB that are important for activity: a cycle of seven residues with three positive charges due to Dab and that contains a hydrophobic domain, D-Phe-Leu, in positions 6 and 7; a linear tripeptide with two positive charges due to Dab; and a middle-length hydrophobic N-terminal chain. Previously reported biophysical studies have shown that sp-B interaction with phospholipid vesicles is analogous to the interaction of PxB.[21,22] Both PxB and sp-B bind to anionic membranes and induce the formation of vesicle−vesicle contacts and selective lipid exchange. sp-C contains a modification in the order of residues 6 and 7, thus breaking the hydrophobic domain of the cycle (Table 1). This domain is important for peptide activity in the membrane.[23,24] sp-C has been shown to interact with anionic vesicles inducing lipid exchange but is not as selective as PxB or sp-B; that is, phosphatidylcholine phospholipids can cross sp-C membrane contacts but not sp-B or PxB contacts.[21] In order to determine the influence of the peptide charges on the interaction, analogue sp-D has been designed and synthesized (Table 1). sp-D contains two residues of l-α,γ-diaminopropionic acid (Dap) in positions 1 and 8. Dap residues have a p$K_a$ of approximately 8.5 as already described[25] and at pH 8.0 will confer upon the peptide a much lower cationic character compared to PxB (the p$K_a$ of Dab is 9.45). Finally, PxB-np is a derivative of PxB obtained by enzymatic treatment. PxB-np has no antibiotic action on Gram-negative bacteria, although it binds LPS and permeabilizes the bacterial membrane to hydrophobic antibiotics.[7,26] This property has been used to develop peptide conjugates for coadministration with otherwise inactive antimicrobial agents.[18]

This work examines the interaction of PxB and PxB analogues with different lipid monolayers that mimic the bacterial membranes. The outer leaflet of the outer membrane (OM) of Gram-negative bacteria is simulated with monolayers of LPS or its lipid anchoring portion, lipid A. The cytoplasmic or inner membrane (IM) is predominantly negatively charged, and monolayers of POPG have been chosen as a model. Insertion of the peptides into the different monolayers has been determined by the Langmuir trough technique, maintaining constant either the surface pressure or the area. In addition, morphological changes in the monolayer upon peptide insertion have been observed by Brewster angle microscopy (BAM) of lipid films after peptide insertion. The results are correlated with the ability of the peptides to induce lipid exchange between membranes, with PxB activity taken as a reference.

## Experimental Section

**Chemicals.** Polymyxin B sulfate salt (PxB), PxB nonapeptide (PxB-np), poly(L-lysine) hydrochloride (MW = 15 000−30 000), lipopolysaccharide (LPS) and lipid A, both from *Salmonella enterica* serotype minnesota Re 595 (Re mutant), Trizma base (Tris), monosodium phosphate monohydrate, and disodium phosphate heptahydrate were purchased from Sigma−Aldrich (St Louis, MO). 1,2-Diacyl-*sn*-glycero-3-phospho-1-*rac*-glycerol sodium salt from egg yolk lecithin (egg PG), 1-palmitoyl-2-oleoylglycero-*sn*-3-phosphoglycerol (POPG), and 1-palmitoyl-2-oleoylglycero-*sn*-3-phosphatidic acid (POPA) were from Avanti Polar Lipids (Alabaster, Ala). 1-Hexadecanoyl-2-(1-pyrenedecanoyl)glycero-*sn*-3-phosphoglycerol (pyPG) and 1-hexadecanoyl-2-(1-pyrenedecanoyl)glycero-*sn*-3-phosphate (pyPA) were purchased from Molecular Probes (Eugene, OR); the latter was obtained by custom-made synthesis. *N*-Fluorenylmethoxycarbonyl- (Fmoc-) protected amino acids, namely, Fmoc-Dab(Boc)-OH, Fmoc-Dap(Boc)-OH, Fmoc-Cys(Trt)-OH, Fmoc-Thr($^t$Bu)-OH, Fmoc-d-Phe-OH, and Fmoc-Leu-OH, were purchased from Bachem (Bubendorf, Switzerland) and Fluka (Buchs, Switzerland). Chemical reagents *N*,*N*-diisopropylcarbodiimide (DIPCDI), *N*-hydroxybenzotriazole (HOBt), and trifluoroacetic acid (TFA) (BioChemika quality) as well as nonanoic acid were also from Fluka (Buchs, Switzerland). Rink amide resin was purchased from Novabiochem (Läufelfingen, Switzerland). Chloroform/methanol (HPLC grade, Fisher Scientific) was used as the spreading solvent for all lipids. Water was doubly distilled and deionized (Milli-Q system, Millipore Corp.).

**Peptide Synthesis and Purification.** Peptide synthesis was performed manually following standard Fmoc/$^t$Bu procedures with DIPCDI/HOBt activation on Rink amide resin.[27] Once the sequence was assembled, cleavage of the peptides from the resin was carried out by acidolysis with TFA/triisopropylsilane/water (95:3:2, v/v) for 90 min. TFA was removed via $N_2$ stream, and the oily residue was treated with dry diethyl ether to obtain the peptide precipitate. The solid peptide was isolated by centrifugation. This process was repeated three times. The homogeneity of peptide crudes was assessed by analytical HPLC on Nucleosil C18 reverse-phase columns (4 × 250 mm, 5 μm particle diameter, and 120 Å porous size). Elution was carried out at 1 mL·min$^{-1}$ flow with mixtures of $H_2O$/0.045% TFA and acetonitrile/0.036% TFA and UV detection at 220 nm. Peptides were subsequently purified by preparative HPLC on a Waters Delta Prep 3000 system with a Phenomenex C18 (2) column (250 × 10 mm, 5 μm) eluted with $H_2O$/acetonitrile/0.1% TFA gradient mixtures and UV detection at 220 nm. Cyclization of peptides through disulfide bonds was carried out in 100 mM ammonium bicarbonate aqueous solutions with pH adjusted to 10 by addition of aqueous concentrated ammonia (32%). Final purity was greater than 95%. Peptides were characterized by amino acid analysis with a Beckman 6300 analyzer and by matrix-assisted laser desorption ionization time of flight (MALDI-TOF) mass spectrometry with a Bruker model Biflex III.

**Kinetics of Insertion into Monolayers.** Monitoring the insertion of peptides into lipid monolayers, either at constant pressure or at constant area, is a sensitive tool for studying lipid/peptide interactions.[28] Insertion experiments were conducted at 24 °C on a computer-controlled monolayer system KSV5000 (KSV, Helsinki, Finland). To avoid carryover of lipid and

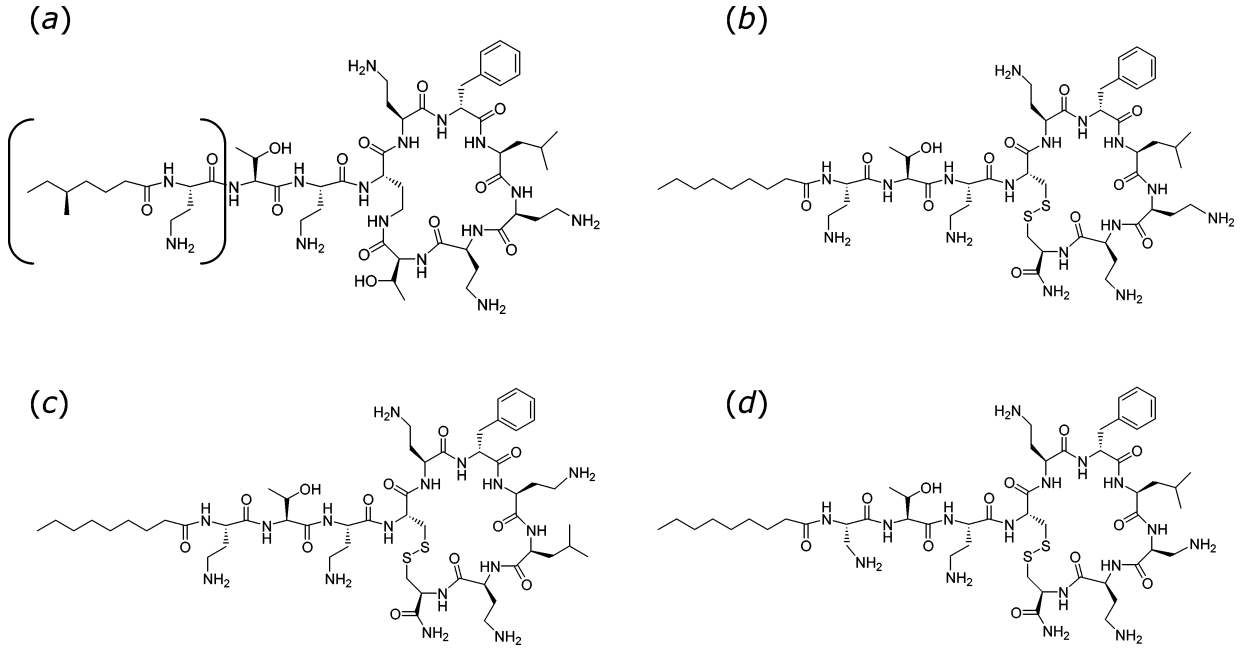


**Figure 1.** Molecular structures of the peptides used in this study: (a) PxB (the structure of PxB nonapeptide lacks the fragment shown in parentheses), and the synthetic analogues (b) sP-B, (c) sP-C, and (d) sP-D.

peptides, the polytetrafluoroethylene (PTFE, Teflon) trough and the Wilhelmy platinum plate were thoroughly cleaned with hot double-distilled water at >75 °C. For experiments at constant surface pressure, the trough consisted of a cylindrical compartment (volume 40 mL, surface area 38.5 $cm^2$) and a rectangular compartment (200 mL, 7.5 × 21.5 cm) connected by a surface canal of etched glass (3 mm with less than 1 mm depth). The platinum plate was set up in the cylindrical compartment for continuous monitoring of the surface pressure. The two compartments were filled with 10 mM Tris, pH 8.0 (40 mL + 200 mL), and with the movable barrier placed close to the canal in the rectangular compartment, a lipid monolayer was deposited to the desired pressure. With the surface pressure stable (for at least 5 min) at a constant preset value, a known aliquot of peptide was then injected in the subphase of the small compartment, with continuous stirring, and the change in trough area to maintain the surface pressure at the preset value was monitored as a function of time. This experimental setup allows us to reduce the amount of peptide needed, since only the monolayer diffuses through the narrow surface canal, without mixing of the subphases from the two compartments. Kinetics of insertion at constant area were also monitored as an increase in the surface pressure by use of a cylindrical trough (5 cm diameter or 19.6 $cm^2$ area) containing stirred aqueous phase (30 mL) with 10 mM Tris at pH 8.0. The peptide was added without disturbance of the monolayer via an inlet port in the trough, and the surface pressure was continuously recorded by the KSV balance.

**Compression Isotherms and Compressibility Modulus.** Pressure/area curves of monolayers were performed with a fully automated monolayer system (NIMA Technology, Coventry, England) equipped with a pressure sensor PS4 and a software trough, enclosed in a Plexiglas box to reduce surface contamination. The surface pressure ($\pi$) of the lipid monolayer was measured by the Wilhelmy method, with a sand-blasted platinum plate connected to an electrobalance. The PTFE trough (surface area 525 $cm^2$, volume 250 $cm^3$) and the plate were thoroughly cleaned before each run with hot water to avoid carryover of lipid or peptide. Lipid solution was prepared by dissolving the mixture in chloroform/methanol (10/1 v/v) to a concentration in lipid of 1 mg/mL. Monolayers were formed by applying small drops of the spreading solutions on the 10 mM Tris buffer subphase (pH 8.0) with a microsyringe (Hamilton Co., Reno, NV). After 30 min, allowing for solvent evaporation and stabilization of the monolayers, they were continuously compressed (symmetrical compression) with an area reduction rate of 20 $cm^2 \cdot min^{-1}$. The films were compressed up to their collapse pressure. Standard deviation was typically ±0.5%. Experiments were done at 24 °C.

The compressibility modulus is defined as

$$C_s^{-1} = -A(\partial\pi/\partial A)_T$$

Its value can be used to characterize the phase of a monolayer, according to Davies and Rideal.[29] The spreading curve ($\pi/A$) shows different regions that correspond to different phases of the monolayer: gaseous, liquid expanded (LE), liquid intermediate (LI), and liquid condensed (LC). In the liquid expanded film, $C_s^{-1}$ ranges between 12.5 and 50 $mN \cdot m^{-1}$; for the liquid intermediate phase, $C_s^{-1} < 100$ $mN \cdot m^{-1}$; while for the liquid condensed phase, $100 < C_s^{-1} < 250$ $mN.m^{-1}$.

**Brewster Angle Microscopy.** The different topographic structures of the monolayers were observed with a commercial miniBAM, manufactured by NFT (Göttingen, Germany), mounted on the NIMA Langmuir film balance previously described. This model uses a class IIIb laser of 30 mW, emitting *p*-polarized light of $\lambda = 660$ nm. BAM examined films do not contain added fluorescent probes. The air−monolayer−water interface was illuminated at 52−54° by a laser beam polarized in the plane of incidence (*p*-polarized), and a lens system focused an image onto a charge-coupled device (CCD) camera. The CCD camera converts the reflectivity signal from the sample into a video image. Principles, and a detailed description of the BAM technique, have been described elsewhere.[30] The purity of the surface was controlled by surface tension measurements during compression of an uncovered subphase. In all cases the surface pressure obtained in these blank tests was less than 0.1 $mN \cdot m^{-1}$; that is, on the order of experimental accuracy. BAM studies were performed to visualize possible impurities as well. All the experiments were carried out at a temperature of 24 °C.

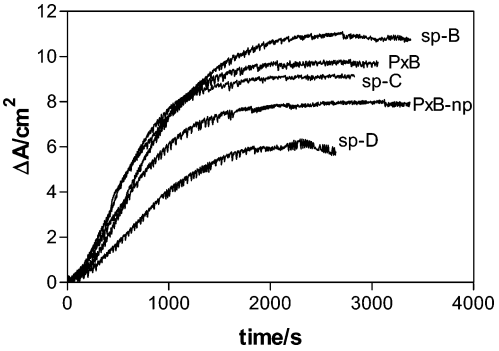


**Figure 2.** Area increase after injection of PxB and analogues into an aqueous subphase underneath a monolayer of LPS from *Salmonella enterica* serotype minnesota Re 595 at a constant surface pressure of 20 mN·m$^{-1}$. Time zero corresponds to the moment of peptide injection. Subphase is 10 mM Tris, pH 8.0, at 24 °C. Peptide concentration is 0.25 $\mu$M.

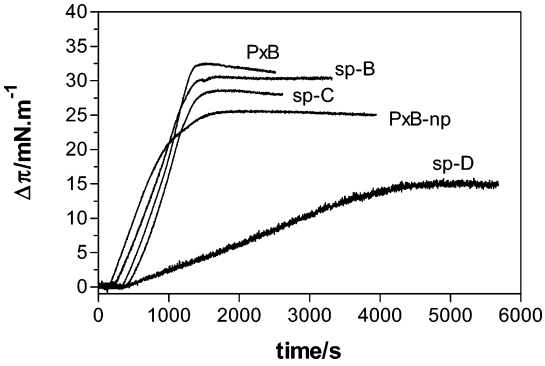


**Figure 3.** Change in surface pressure after injection of PxB and analogues into an aqueous subphase underneath a monolayer of LPS from *Salmonella enterica* serotype minnesota Re 595 at constant area. Other conditions are as in Figure 2.

**Fluorescence Assay for Lipid Mixing.** The exchange of lipid molecules between vesicles induced by the different peptides was assessed as described previously.[31,32] Briefly, transfer of pyrene-labeled phospholipids as donor vesicles to a more than 100-fold excess of unlabeled phospholipid vesicles as acceptors was measured. Emission from vesicles containing 30% pyrene-phospholipid is dominated by the excimer band at 480 nm, and the intensity of the monomer band, at 395 nm, increases as the probe is diluted due to exchange with excess unlabeled vesicles in contact. Experiments were done at 24 °C in 10 mM Tris buffer at pH 8.0 or in phosphate buffer at different pH values as indicated. Fluorescence measurements were carried out on an AB-2 spectrofluorometer (SLM-Aminco) with constant stirring. Typically, the slit widths were kept at 4 nm each and the sensitivity (photomultiplier tube voltage) was adjusted to 1% for the Raman peak corresponding to the same excitation wavelength from the buffer blank. Fluorescence emission was monitored at 395 nm (with excitation at 346 nm) corresponding to the monomer emission. Unilamellar lipid vesicles used for the exchange experiments were prepared with POPG or POPA alone or with 30% pyPG or pyPA, as described elsewhere.[32]

## Results

**Peptide Insertion into Monolayers of LPS.** The penetration of the different peptides into monolayers of LPS gives information that can be significant to understand the mechanism of action of the peptide on the OM of Gram negative bacteria. The experiments can be conducted in two ways: maintaining a constant pressure or at constant area. In the first set of experiments (Figure 2), the film pressure was kept constant at a preset value of 20 mN·m$^{-1}$, and the insertion was followed by observing the increase in area of the monolayer. The subphase concentration of the peptides was 0.25 $\mu$M, which is in the range of the minimum inhibitory concentration (MIC) for PxB on Gram-negative bacteria.[7,12] PxB readily inserted in the LPS monolayer, reaching a plateau at 30 min after injection of the peptide. The maximum increase in area was 9.7 cm$^2$, which corresponds to 19 Å$^2$·molecule$^{-1}$ if only the lipid is considered. The synthetic peptides showed different degrees of penetration depending on their structure and net charge (see structures in Figure 1). The higher increase in surface area corresponded to sp-B, with an increment of 11.0 cm$^2$ obtained after the steady-state plateau was reached (approximately 35 min after injection). This synthetic peptide had a higher degree of insertion than the parent compound PxB. Synthetic peptide sp-C, with the mutation in the hydrophobic domain of the cycle,

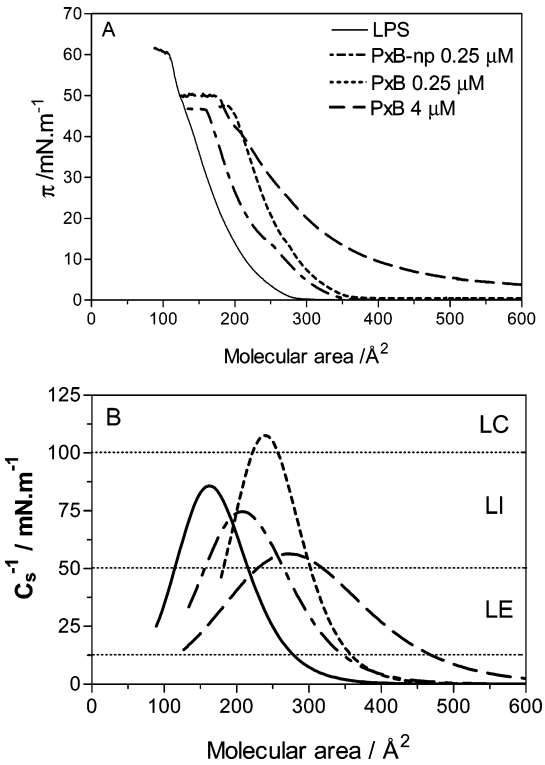


**Figure 4.** (A) Surface pressure−area isotherms for LPS spread at the air/water interface of 10 mM Tris, pH 8.0, alone, with PxB, or with PxB-np. Molecular areas were calculated with respect to the lipid. (B) Compressibility modulus ($C_s^{-1}$) of the same isotherms. The dotted lines mark the regions of gaseous, LE, LI, and LC phases.

was slightly below PxB. PxB-np induced an important expansion of the monolayer, indicating that the deacylated derivative inserts into the LPS film, although the maximum area increase was slightly lower (around 8 cm$^2$). Finally, sp-D, with a lower cationic charge, had the lowest degree of insertion.

Similar penetration assays were carried out at constant area by first spreading the LPS film at 20 mN·m$^{-1}$ and then injecting the peptides, with subsequent peptide insertion resulting in a pressure increase. As shown in Figure 3, under these conditions the differences between the peptides were minimized, with similar increases in surface pressure obtained for PxB, sp-B, and sp-C. This is not surprising given the high affinity of the cationic peptides for LPS: in the constant area experiments, the surface pressure increases upon peptide insertion, resulting in a more tightly packed film. When the surface pressure increases approximately 30 mN·m$^{-1}$, the total pressure is 50 mN·m$^{-1}$, which corresponds to the collapse of the monolayer

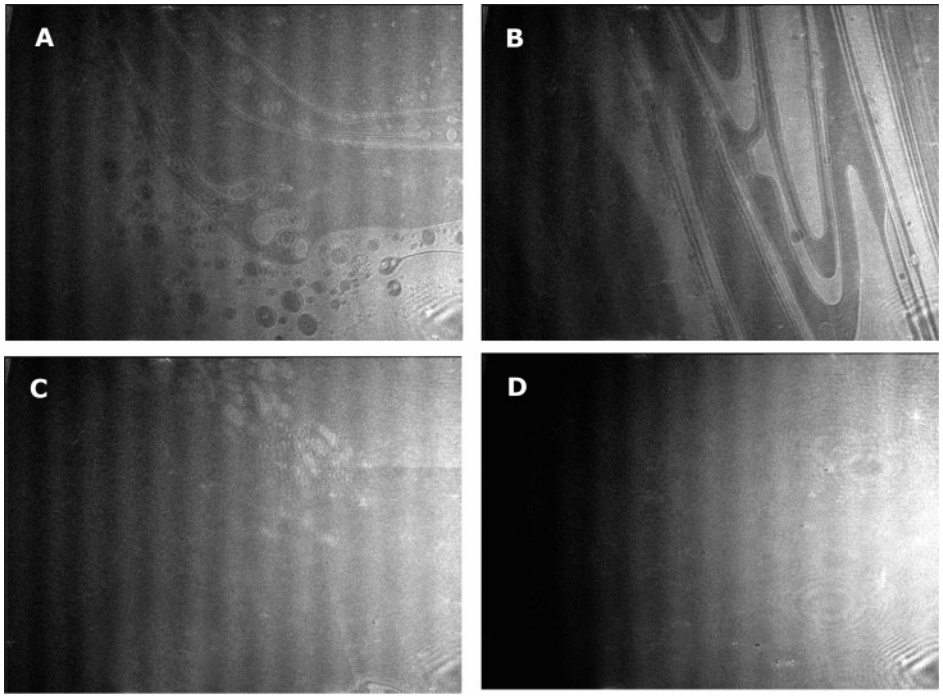


**Figure 5.** Visualization by BAM of LPS monolayers spread on the air/water interface on a subphase of 10 mM Tris at pH 8.0 and 24 °C: (A) 0, (B) 0.5, (C) 2, and (D) 10 mN·m$^{-1}$, homogeneous monolayer.

(shown later), thus preventing the insertion of more peptide. Lower levels of insertion were obtained for PxB-np and specially for sp-D, in good agreement with the results obtained at constant pressure (Figure 2).

**Structural Characteristics of LPS Monolayers.** The surface morphology of these insertion events was monitored by Brewster angle microscopy (BAM). LPS monolayers were compressed to obtain the pressure/area curves (isotherms), and changes in film morphology were simultaneously monitored. Figure 4A shows the isotherms of LPS monolayers spread at the air/water interface on a subphase of buffer alone or containing peptide. As already observed in the kinetic experiments (Figure 2), addition of PxB or PxB-np led to an increase of the area of LPS monolayers: the isotherms were shifted to the right due to insertion of the peptide. A closer examination indicated that, as a result of the insertion, LPS packing was drastically modified. Compressibility modulus ($C_s^{-1}$) calculations are shown in Figure 3B. According to $C_s^{-1}$ analysis, LPS monolayer is in a liquid expanded (LE) phase at molecular areas in the range 215−280 Å$^2$·molecule$^{-1}$, or surface pressures between 0.7 and 7 mN·m$^{-1}$, and adopts a liquid intermediate (LI) phase at higher surface pressures until reaching the collapse point at 60 mN·m$^{-1}$. Thus, the film at 20 mN·m$^{-1}$ used for the kinetic experiments is in the LI phase. In the LI phase, the lipid molecules are very close to each other and the interactions between the chains are large.[33,34] BAM images of the LPS monolayer were taken at different surface pressures (Figure 5). The images clearly indicate that at very low surface pressures, where according to $C_s^{-1}$ calculations the monolayer has not yet reached the LE phase, the film is not homogeneous (Figure 5A), with a coexistence between dark gray domains of gaseous phase and less abundant areas of higher packing of the LPS molecules (lighter color), which probably correspond to LE phase. The domains of LE phase increase in size upon compression (Figure 5B). At around 2 mN·m$^{-1}$ small and bright domains appear, corresponding to some regions of more closely packed LPS molecules or LI phase in a matrix of LE phase (Figure 5C). At surface pressures of 6 mN·m$^{-1}$ and above, a totally homogeneous image is obtained, in agreement with $C_s^{-1}$ calculations that predicted the existence of LI phase until the collapse of the monolayer, which occurs at around 60 mN·m$^{-1}$.

Addition of 0.25 $\mu$M PxB in the subphase underneath a LPS monolayer resulted not only in an expansion of the film (Figure 4A) but also in a closer packing of the molecules, with the formation of LI phase from 300 Å$^2$·molecule$^{-1}$, which corresponds to only 5 mN·m$^{-1}$ (Figure 4B). In addition, at this concentration of PxB, which corresponds to the MIC for most Gram-negative bacteria, $C_s^{-1}$ reaches values above 100 mN·m$^{-1}$, characteristic of LC phase, when the molecular areas are below 260 Å$^2$·molecule$^{-1}$, or at surface pressures higher than 15 mN·m$^{-1}$. LC phase is characterized by a closely packed and rigid arrangement of the lipid components that possess an almost vertical orientation at the air/water interface. This implies that at 20 mN·m$^{-1}$, the surface pressure used in the insertion experiments (Figure 2), LPS is initially in the LI phase but insertion of polymyxin results in a higher packing of the LPS molecules, with a change from LI to LC phase. Representative BAM images of the LPS/PxB monolayer are shown in Figure 6. At very low surface pressures, the images show the existence of a heterogeneous film (Figure 6A), with domains of gaseous phase (dark areas) intercalated with areas of more densely packed molecules or LE phase (light color). Compression of the monolayer increases the area corresponding to the LE phase (Figure 6B). Compared to the pure LPS monolayer, the presence of PxB induces a higher order in the film, with a different morphology consisting of bands of condensed and expanded regions, with a higher percentage of the light gray domains of more condensed structure. Further compression of the film results in an increase of LE phase, that still coexists with filamentous regions of gaseous film (Figure 6C, at 0.5 mN·m$^{-1}$). At surface pressures above 2 mN·m$^{-1}$, BAM images show the existence of a homogeneous film (Figure 6D,E), attributed to pure LE phase ($C_s^{-1}$ < 50 mN·m$^{-1}$). At surface pressures above 15 mN·m$^{-1}$, the homogeneous film is sprinkled with bright nuclei of condensation (Figure 6F), denoting the beginning of the monolayer collapse via a nucleation mechanism.[35] Also,

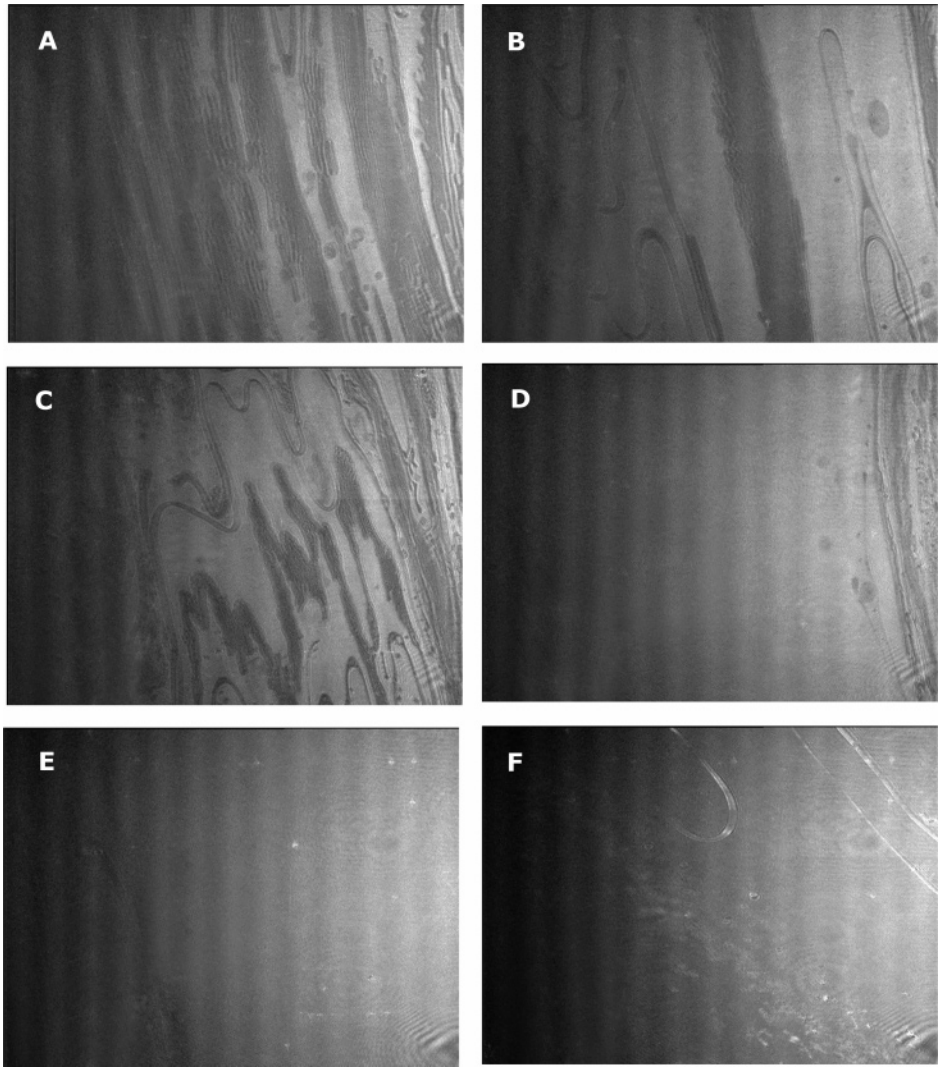


**Figure 6.** Visualization by BAM of LPS monolayers spread on the air/water interface on a subphase containing 0.25 $\mu$M PxB: (A) 0, (B) 0.1, (C) 0.5, (D) 4, (E) 10, and (F) 35 mN·m$^{-1}$, close to collapse. Other conditions are as in Figure 5.

some long stripes are beginning to form, due to the merging together of the nuclei of condensation. The collapse pressure was 46 mN·m$^{-1}$. It is worth mentioning that both LPS and mixed LPS/PxB monolayers are very stable at all surface pressures, with very little hysteresis obtained upon two consecutive compression and expansion cycles (not shown). For example, at 20 mN·m$^{-1}$, the decrease in area in the second compression was only 4−5% for LPS and 3% for the mixed monolayer.

Significant differences were observed when the concentration of PxB in the subphase was severalfold higher than the MIC, for example, 4 $\mu$M. In this case, PxB also inserted in the LPS monolayer, with important increases in area (Figure 4A). However, the compressibility modulus was lower than that of LPS at the same surface pressure, indicating a decrease in the molecular packing of the film. In this case, the LPS/PxB mixed monolayer was mostly in the LE phase throughout compression, with formation of LI only at surface pressures above 15 mN·m$^{-1}$ but without formation of LC phase.

When PxB-np was added to the subphase, it also inserted in the LPS monolayer, although to a lesser extent compared to the same concentration of PxB (Figure 4A). This indicates that not only are the electrostatic interactions important for peptide insertion, but also the hydrophobic interactions between the N-terminal acyl chain of PxB and the fatty acids of LPS play an important role. $C_s^{-1}$ analysis of the $\pi/A$ curve (Figure 4B) indicated that PxB-np containing LPS monolayer was initially in LE phase and adopted the LI state at 260 Å$^2$·molecule$^{-1}$, which corresponds to 10 mN·m$^{-1}$. The monolayer reached collapse without adopting the LC phase. BAM images obtained at different surface pressures were equivalent to the images obtained for LPS/PxB monolayer (not shown).

**Structural Characteristics of Lipid A Monolayers.** Isotherms of pure lipid A are shown in Figure 7. Lipid A is the hydrophobic moiety of LPS, and for *Salmonella enterica* it is composed of a diglucosamine backbone that is phosphorylated in positions 1 and 4′ and acylated by seven hydrocarbon chains ester and amide linked at positions 2, 3 and 2′, 3′. The structural characteristics of a lipid A monolayer were different from that for LPS as deduced from the compression isotherms shown in Figure 7A. Lipid A lacks the sugar portion of LPS, and therefore has lower molecular areas. According to $C_s^{-1}$ calculations (Figure 7B), lipid A monolayers are in a gas phase at surface pressures below 2−3 mN·m$^{-1}$, adopt LE structure between 3 and 14 mN·m$^{-1}$, and have LI structure above this pressure until reaching the collapse phase at about 46 mN·m$^{-1}$. This lower value of the collapse pressure compared to LPS (60 mN·m$^{-1}$) suggests that lipid A monolayer is less stable. BAM images

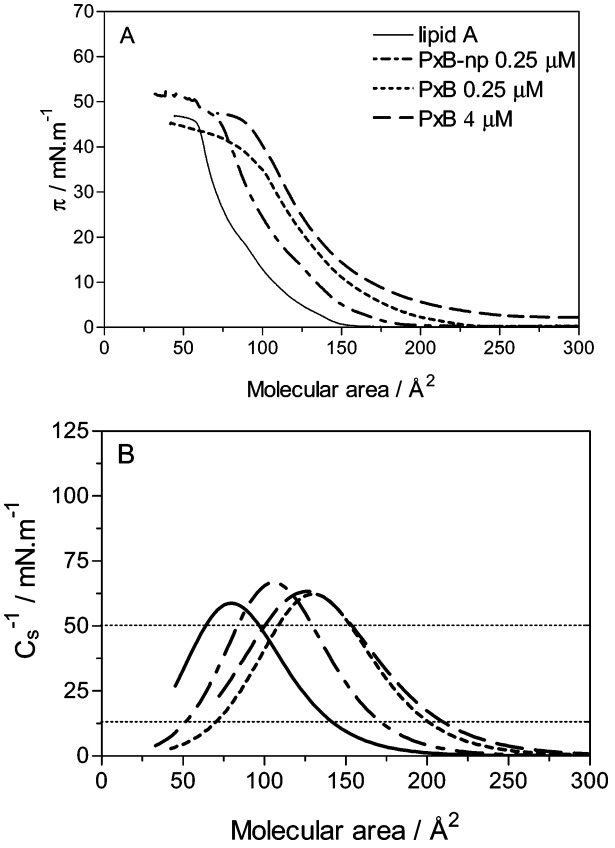


**Figure 7.** (A) Surface pressure−area isotherms for lipid A spread at the air/water interface of 10 mM Tris, pH 8.0, alone, with PxB, or with PxB-np. Molecular areas were calculated with respect to the lipid. (B) Compressibility modulus ($C_s^{-1}$) of the same isotherms.

taken in different regions of the monolayer are shown in Figure 8. The images clearly indicate that at very low surface pressures ($\pi = 0$ mN·m$^{-1}$, Figure 8A) there is coexistence between rounded domains of gas phase (dark color) surrounded by liquid-expanded domains (light color). Upon monolayer compression, the LE domains grow in size at the expense of the gaseous ones (Figure 8B). At surface pressures above 2 mN·m$^{-1}$, the monolayer is mostly in LE phase (Figure 8C) until a homogeneous film of LE phase is formed (Figure 8D). The formation of small round or long stripes of brighter domains at $\pi > 14$ mN·m$^{-1}$ (Figure 8E) is due to the more condensed LI phase. Finally, close to the collapse pressure, we see the formation of condensation nuclei that merge to form long stripes (Figure 8F), as already described for LPS.

When lipid A was extended on a PxB-containing subphase, there was a monolayer expansion as PxB molecules inserted in the lipid A film, as shown in the isotherm in Figure 7A. However, as opposed to LPS binding, insertion of PxB into lipid A induced only small changes in the structural characteristics of the lipid A monolayer, as deduced from the compressibility analysis of the isotherms (Figure 7B). Interestingly, the same results were obtained at low or high concentrations of PxB in the subphase, another difference from the interaction with LPS. BAM images of the lipid A/PxB monolayer at different surface pressures are shown in Figure 9. Images are in good agreement with the conclusions obtained from $C_s^{-1}$ analysis. At very low surface pressures, or high molecular areas, the images are consistent with the coexistence of two phases, a gaseous phase and a more densely packed or LE phase (Figure 9A). However, the morphology of the domains is different than in pure lipid A monolayers, with a longitudinal distribution of intercalated gas and expanded domains induced by PxB. When the area per molecule decreases, but still at very low surface pressure (Figure 9B), the domains of LE phase grow bigger, and at 3 mN·m$^{-1}$ the monolayer is practically homogeneous in the LE phase, with only small rounded domains of the less packed structure (Figure 9C). In the range of surface pressures from 3 to 10 mN·m$^{-1}$ approximately, the monolayer has a homogeneous morphology (Figure 9D at 5 mN·m$^{-1}$). At surface pressures above 10 mN·m$^{-1}$, brighter domains of more condensed phase are formed, which can be attributed to LI phase (Figure 9E, 25 mN·m$^{-1}$). These domains grow in size upon compression, with the formation of nuclei of condensation and long filaments that indicate the beginning of the collapse of the monolayer (Figure 9F).

**Peptide Insertion into Monolayers of POPG.** We carried out insertion studies using POPG monolayers to mimic the inner or cytoplasmic membrane (IM) of the bacteria and the inner leaflet of the OM as well, both rich in anionic phospholipids with unsaturated tails. Upon injection of 0.25 $\mu$M PxB into the subphase underneath a POPG monolayer at a surface pressure of 20 mN·m$^{-1}$, the increase in area was very small (data not shown), compared to the increases obtained in LPS monolayers (Figure 2). Thus, we increased the concentration of peptide to 0.5 $\mu$M in these experiments, resulting in a maximum area increase of 4 cm$^2$ in the case of PxB (Figure 10). Synthetic analogue sp-B showed a higher level of insertion compared to the parent peptide, a behavior similar to the described interaction with LPS film (Figure 2). sp-C kinetics of penetration were comparable to those of PxB. However, although PxB-np penetrated readily into LPS monolayers, it practically did not insert into POPG films at the same pressure (Figure 10). This behavior has already been described for the interaction of PxB-np with anionic monolayers of *Escherichia coli* lipid extract,[36] and it can be attributed to interfacial binding of the peptide to the polar head groups of the phospholipids, without insertion into the monolayer. To test this hypothesis, at the end of the experiment of PxB-np insertion, PxB was injected underneath the monolayer, with almost no further change in surface area (not shown), thus confirming that PxB-np was bound to POPG although it did not insert into the lipid film. sp-D showed a significantly lower level of insertion into POPG compared to the other sinthetic peptides, a result that proves the importance of the five Dab residues for binding and insertion (Figure 10).

**Structural Characteristics of PG Monolayers.** For a better understanding of the interaction of PxB with PG monolayers, the compression isothems of PG alone and in the presence of peptide added to the subphase were obtained and observed by BAM. In these experiments, eggPG was used due to the difficulties of obtaining good BAM images from POPG monolayers. As shown in Figure 11A, in the presence of PxB a shift to higher area per molecule was detected at all surface pressures up to collapse of the monolayer, thus suggesting that PxB binds and inserts into the monolayer, causing an expansion of the lipid film, and is not desorbed form the monolayer at high surface pressures. This is in agreement with previous studies on the interaction of PxB with monolayers of *Escherichia coli* lipid extract.[36] The stability of the PG monolayers was assessed by two successively taken compression and expansion cycles without reaching collapse, showing a very small hysteresis. On the other hand, when the PG monolayer was spread on a subphase containing PxB-np, the resulting compression isotherm was identical to that of pure PG (Figure 11A), as expected since PxB-np binds only superficially to the lipids without insertion. Compressibility modulus analysis (Figure 11B) indicated that

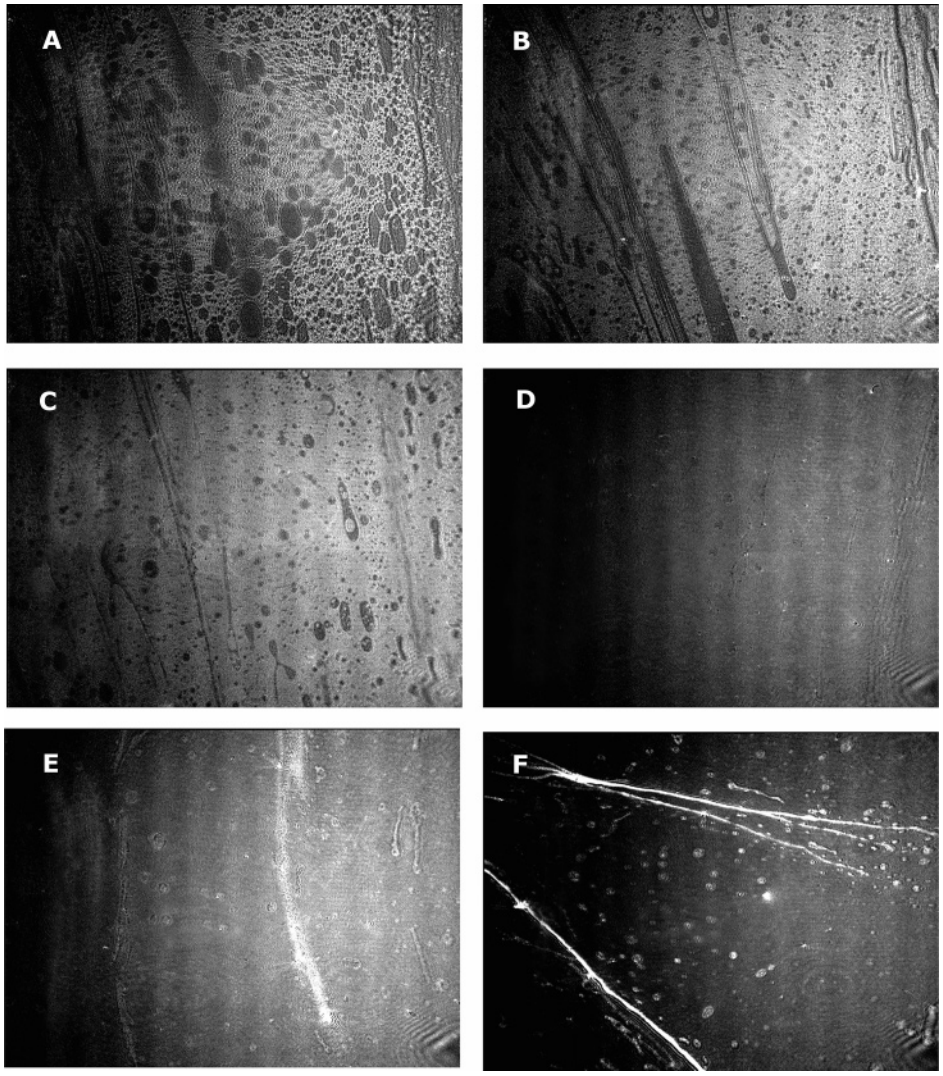


**Figure 8.** Visualization by BAM of lipid A monolayers spread on the air/water interface on a subphase of 10 mM Tris at pH 8.0 and 24 °C: (A) 0, (B) 0.5, (C) 3, (D) 10, (E) 25, and (F) 42 mN·m$^{-1}$.

eggPG monolayers were more fluid than LPS monolayers, because LC or even LI phases were not formed. This is related to the low transition temperature of eggPG (around −2 °C), well below the temperature of the experiments. PG monolayers adopted the LE phase at 2 mN·m$^{-1}$, and were in this state until reaching collapse at ≈44 mN·m$^{-1}$. In the presence of PxB, the expanded monolayer adopted the LE phase at slightly higher surface pressures (3.5 or 5 mN·m$^{-1}$ depending on the concentration of peptide in the subphase; see Figure 11B), indicating that PxB slightly decreased the packing of the monolayer. This is further confirmed by the maximum $C_s^{-1}$ values, which are lower at 0.5 $\mu$M than at 0.25 $\mu$M PxB in the subphase. BAM images were taken at different surface pressures during compression, and representative examples are shown in Figure 12. It can be seen that at the beginning of compression, when the surface pressure is practically zero (Figure 12A), the monolayer had areas of gaseous phase (dark gray domains) that are filamentous in shape, but already at this low pressure most of the lipid is in the more condensed LE phase (light color). Above 1−2 mN·m$^{-1}$ the film became totally homogeneous in the LE phase (Figure 12B) and remained like this through all compression up to collapse, when bright filaments were formed (Figure 12C). Images obtained in the presence of 0.25 $\mu$M PxB were indistinguishable from the images corresponding to pure PG at the same surface pressures (Figure 12 A′−C′), a result that is consistent with the compressibility modulus calculations. Finally, BAM images corresponding to a higher concentration of PxB in the subphase (0.5 $\mu$M PxB) showed a homogeneous film at all surface pressures (not shown), which is expected given the fact that the surface pressure at the beginning of compression was already high (2 mN·m$^{-1}$) due to insertion of PxB.

**Phospholipid Exchange Induced by the Peptides.** PxB ability to induce vesicle−vesicle contacts and exchange of phospholipids between vesicles has been described in detail[31,32] and has been proposed as the basis of the antibiotic action of this and related antibiotics on Gram-negative bacteria.[14−16] One of the key features of vesicle−vesicle contacts is the selectivity for a certain type of molecules: phospholipids with one anionic charge (i.e., PG) are rapidly exchanged through the contacts, but dianionic phospholipids (i.e., PA) are excluded. We have previously described that sp-B induces lipid exchange in a mixture of PG/pyPG (7:3) vesicles with 125-fold excess of PG vesicles, and the efficiency of transfer is comparable to that of PxB.[22] In the same paper, we also showed that sp-B lipid exchange is selective for monoanionic phospholipids, such as PG, and that exchange of dianionic phospholipids such as PA is much lower. We now extend these results to the other analogues (Figure 13). sp-C induces significant exchange of pyPG, starting at very low peptide concentrations at the interface (Figure 13A), whereas exchange of pyPA is very low (Figure

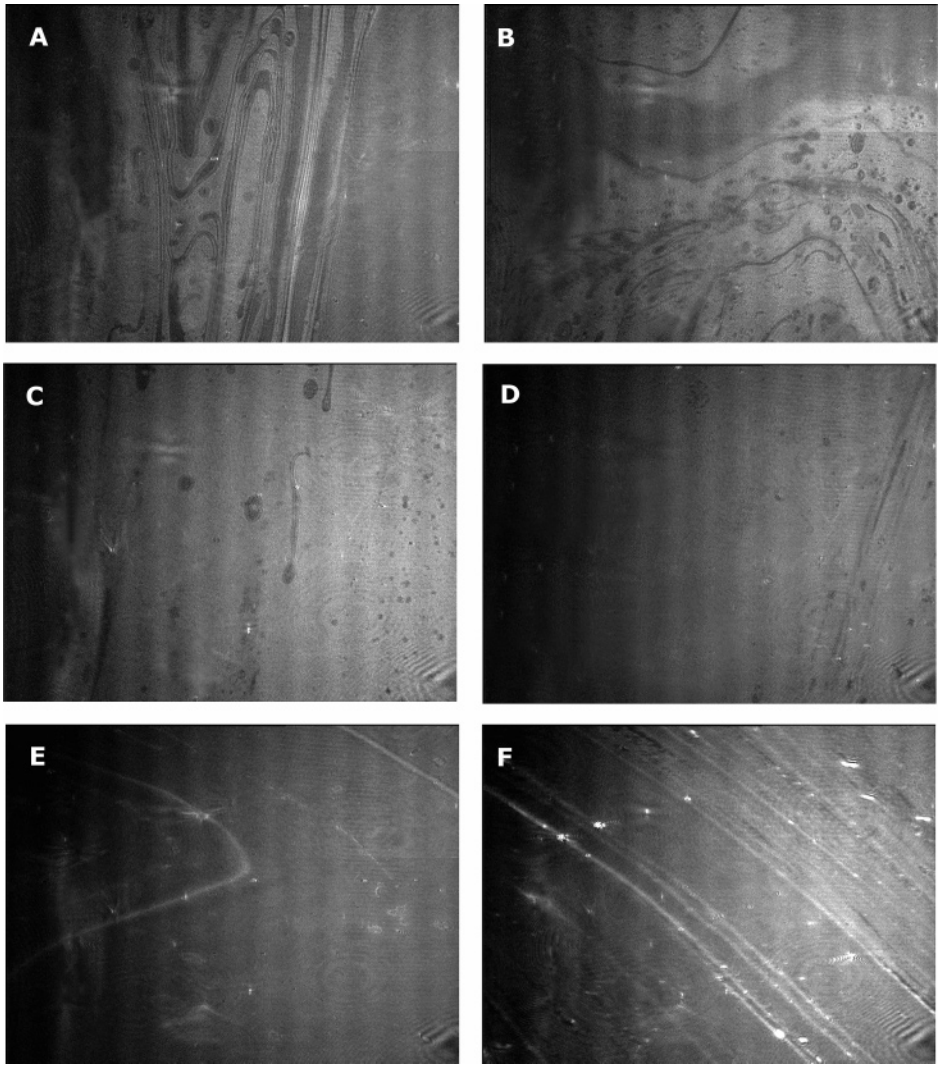


**Figure 9.** Visualization by BAM of lipid A monolayers spread on the air/water interface on a subphase containing 0.25 $\mu$M PxB: (A) 0, (B) 0.5, (C) 3, (D) 5, (E) 25, and (F) 43 mN·m$^{-1}$. Other conditions are as in Figure 8.

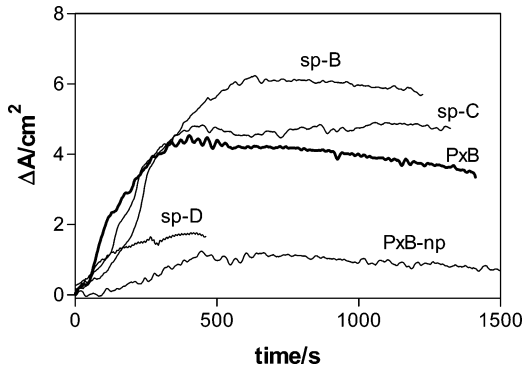


**Figure 10.** Area increase after injection of PxB and analogues into an aqueous subphase underneath a monolayer of POPG at a constant surface pressure of 20 mN·m$^{-1}$. Time zero corresponds to the moment of peptide injection. Peptide concentration is 0.5 $\mu$M. Subphase is 10 mM Tris, pH 8.0, at 24 °C.

13B). On the other hand, sp-D is much less effective, with only a small increase in pyPG monomer fluorescence and no exchange of pyPA. As controls in these experiments, we have used polylysine, which induces unspecific lipid mixing due to vesicle fusion. Results in Figure 13 show that polylysine has the same effect in both types of anionic vesicles. The second control is PxB-np: the deacylated derivative of PxB is not able to induce vesicle−vesicle contacts and lipid exchange,[21,22] therefore no changes in pyrene monomer fluorescence are detected.

## Discussion

**Interaction with Monolayers of OM Lipids.** To better understand the mechanistic aspects of the antibiotic activity of PxB on Gram-negative bacteria, it is important to utilize the lipids composing the outer and the inner membranes of this type of bacteria. We have used lipid monolayers at the air/water interface as a simplified reconstitution model. First, monolayers of LPS or lipid A from *Salmonella enterica* (Re mutant) have been prepared and their physicochemical characteristics have been studied by obtaining compression isotherms (Figures 4 and 7) and BAM images (Figures 5 and 8). At biologically relevant surface pressures, for example, 20 mN·m$^{-1}$ (this pressure has been selected for the insertion experiments), both monolayers are in the liquid intermediate phase (LI), with important interactions between the acyl chains of the molecules. BAM images of LPS and lipid A monolayers at this surface pressure are consistent with an homogeneous film. Insertion experiments at constant pressure (Figure 2) or at constant area (Figure 3) indicate that PxB and the different PxB analogues are able to bind LPS, inserting between the molecules and expanding the lipid film. Both electrostatic and hydrophobic interactions are

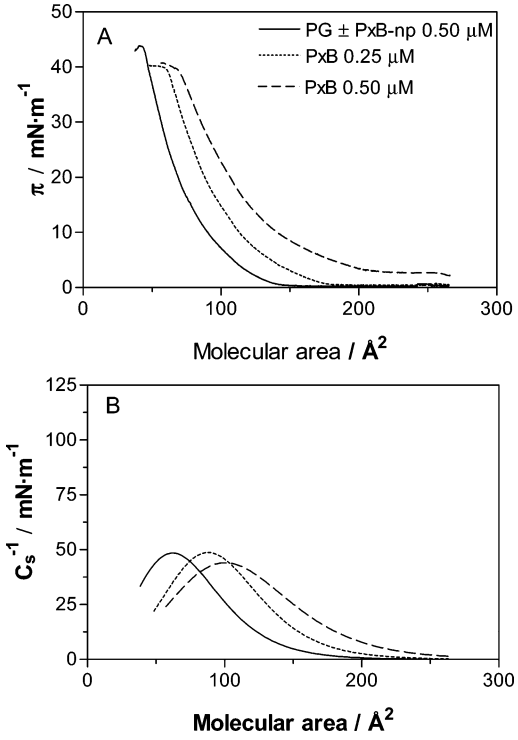


**Figure 11.** (A) Surface pressure−area isotherms for eggPG spread at the air/water interface of 10 mM Tris, pH 8.0, alone, with PxB, or with PxB-np. Molecular areas were calculated with respect to the lipid. (B) Compressibility modulus ($C_s^{-1}$) of the same isotherms.

important for peptide binding and insertion. PxB, sp-B, and sp-C have five positive charges due to Dab residues that are mostly protonated at pH 8.0, whereas sp-D has an overall lower positive character at the pH of the experiments, given the p$K_a$ of Dap (≈8.5), and thus it has a lower affinity for binding to anionic LPS and lipid A. However, electrostatically driven binding is not enough to explain PxB−LPS interaction, as also reported by others;[12,24,37] other effects such as hydrophobic interactions also play a role. PxB has two hydrophobic regions: the N-terminal acyl chain and the D-Phe-Leu domain of the cycle (Figure 1). Results shown here indicate that both are important for peptide insertion into the LPS film. For example, PxB-np, without the acyl chain, has a lower level of insertion, and sp-C, with the hydrophobic domain of the cycle D-Phe$^6$-Leu$^7$ truncated, also shows lower binding affinity (Figures 2 and 3). BAM images of the PxB-containing LPS and lipid A monolayers show that PxB induces important changes in the film morphology. PxB insertion results in a higher packing of the monolayer, with the formation of more condensed phases at lower surface pressures. These results are in good agreement with previously reported data based on atomic fluorescence microscopy (AFM)[38] and epifluorescence microscopy.[39] The effect on LPS packing is more prominent when PxB concentration in the subphase is around the MIC for Gram-negative bacteria (0.25 $\mu$M). This argues against membrane breakdown as the sole mechanism of action of this antibiotic: interaction with LPS is a way of crossing the OM, but bacterial killing involves other targets.[12,13] An estimate of the LPS/PxB ratio at the interface can be deduced from the insertion experiments at constant pressure (20 mN·m$^{-1}$, Figure 2). The structure of PxB at the lipid interface has been previously determined from NMR data and molecular modeling calculations.[23] According to these data, PxB adopts a well-defined structure at the anionic interface. The structure with lowest energy is quite flat, with the aromatic ring of d-Phe$^6$ oriented over the methyl groups of Leu$^7$ and with a kink between residues 1−3 in the linear part. If this structure lies perpendicular to the interface, with the acyl chain parallel to the fatty acids of LPS or lipid A and the cationic residues close to the anionic charges of the lipid monolayer, the estimated area occupied by each PxB molecule is 90−100 Å$^2$. If we assume similar area is occupied by each LPS molecule before and after PxB insertion, the maximum area increase in Figure 2 corresponds to an LPS/PxB ratio of 2:1, slightly above the charge compensation value of 1.25:1 obtained by isothermal titration, considering that each LPS molecule bears four negative charges and PxB has five positive charges.[37] On the other hand, if we assume that PxB lies with the long axis parallel to the interface and with the acyl chain inserted into the lipid film, the estimated area per molecule is 300 Å$^2$, which represents an LPS/PxB ratio of 6.5:1. We prefer the first possibility, also proposed by Tsubery et al.[24] for PxB bound to LPS[4] in this work, the authors propose that the hydrophobic segment D-Phe-Leu and the N-terminal fatty acid interact with the aliphatic chains, and the positive residues of Dab interact with the anionic phosphate groups of lipid A.

**Interaction with Monolayers of IM Lipids.** Data reported here show that synthetic analogues sp-B and sp-C bind LPS with high efficiency and intercalate between the LPS molecules that form the outer leaflet of the OM. This is a necessary first step to enter in the periplasmic space by a mechanism known as self-promoted uptake.[11,40] However, binding to LPS is not sufficient for bacterial killing. For example, PxB-np, with good affinity for LPS and lipid A, has no antibiotic effect.[7] Recent data indicate that bacterial killing requires the simultaneous interaction of PxB with the outer and inner or cytoplasmic membranes of Gram-negative bacteria.[12,14,41] The internal monolayer of the OM, as well as the IM of Gram-negative bacteria, contain anionic phospholipids, such as phosphatidylglycerol (PG). PxB mechanism of action is based on osmotic imbalance due to exchange of anionic phospholipids through inner and outer membrane contacts formed by PxB.[14−16] This antibacterial mechanism has major implications in bacterial resistance, since bacteria would not be susceptible to generate stable genetic resistance. In fact, acquisition of resistance by a sensitive microbial strain against polymyxins and other antibiotic peptides is surprisingly improbable.[2,6,17,18] Data presented here show that PxB and the synthetic PxB analogues with five positive charges and the N-terminal acyl chain of nonanoic acid, sp-B and sp-C, are able to bind and insert into monolayers of phosphatidylglycerol, with significant increases in the mean molecular areas (Figure 10). sp-B has an insertion efficiency above that of PxB. Comparing these insertion processes with the absence of penetration shown by PxB-np allows us to dissect the processes of binding and insertion. The lack of acyl chain in PxB-np, together with a lower number of cationic charges (Dab-1 is not present), prevents insertion of the peptide, a process that is mainly driven by hydrophobic interactions between the fatty acids of the phospholipids and the acyl chain of the peptide. However, our data suggest that PxB-np binds superficially to the lipid interface without insertion, therefore reducing the degree of insertion of PxB added afterward (see Results); the same behavior was described for the interaction with monolayers of *Escherichia coli* lipid extracts.[36] These results imply that binding to POPG is driven by electrostatic forces of attraction. This is further confirmed by results with sp-D. This peptide has a lower content in positive charges at pH 8, compared to PxB, sp-B, sp-C, and even PxB-np, but maintains the C9 acyl tail at the N-terminus. sp-D inserts into POPG monolayers (Figure 10), but the increase in surface area

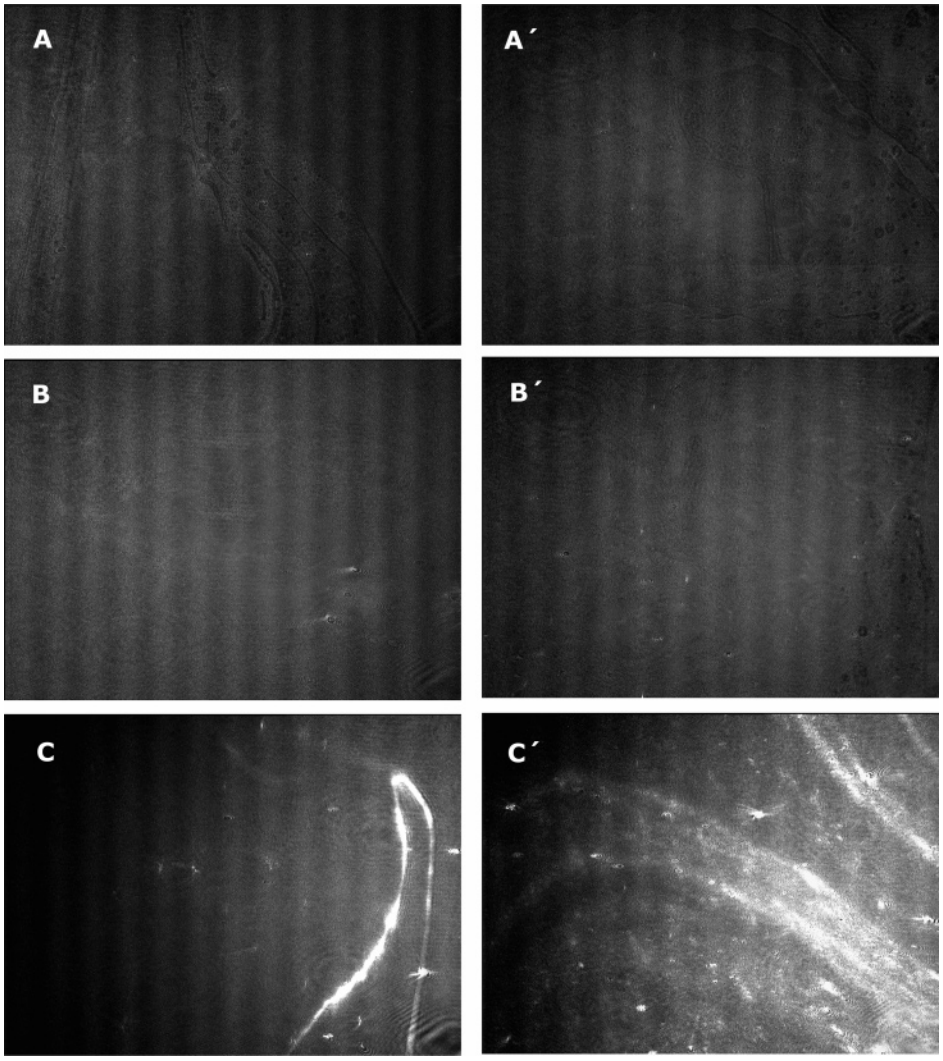


**Figure 12.** Visualization by BAM of eggPG monolayers spread on the air/water interface on a subphase of 10 mM Tris alone (A−C) or containing 0.25 $\mu$M PxB (A′−C′). Surface pressures: 0.2 (A, A′), 10, (B, B′), and 38 mN·m$^{-1}$ (C, C′). Other conditions are as in Figure 11.

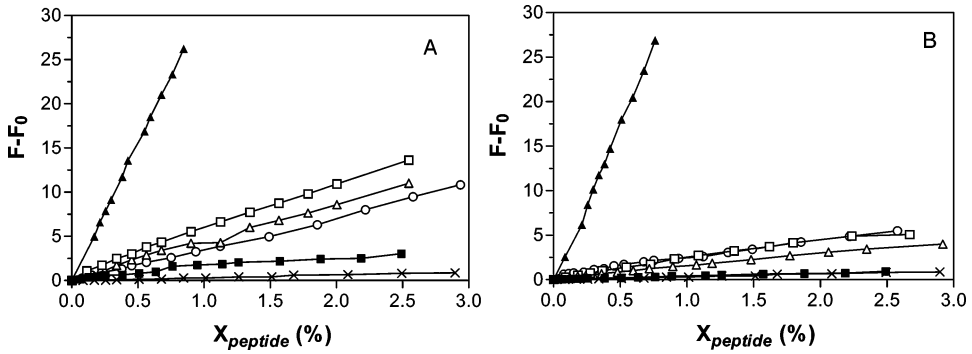


**Figure 13.** Fluorescence intensity of pyrene monomer as a function of peptide mole fraction in mixed vesicles of (A) pyPG with POPG; (B) pyPA with POPA. Peptides: PxB (□); sp-B (△); sp-C (○); sp-D (■); PxB-np (×); polylysine (▲). Bulk lipid concentration is 1.67 $\mu$M for py vesicles and 213.33 $\mu$M for unlabeled acceptor vesicles, in 10 mM Tris, pH 8.0. Excitation 346 nm, emission 395 nm. Results corresponding to PxB and sp-B are from ref 22.

is smaller than those induced by sp-B and sp-C, indicating lower affinity. BAM images of PG monolayers are consistent with a fluid monolayer, as expected due to its high content in unsaturated fatty acids of this phospholipid. Insertion of PxB results in important expansion of the monolayer (Figure 11) but does not significantly modify the morphology of the lipid film, as deduced from compressibility modulus analysis and BAM images (Figure 12). Similarly, previous studies on the interaction of PxB with lipid vesicles of *E. coli* lipids show that at concentrations around the MIC, PxB has no significant effect on membrane microviscosity.[42]

**Contact Formation and Lipid Exchange between Unilamellar Vesicles.** Once the peptides are bound to and inserted into the anionic phospholipid interface, it is important to know whether they are functional; that is, if they are able to induce the formation of vesicle−vesicle contacts and phospholipid exchange. We have already shown that PxB, but not PxB-np, forms contacts between anionic vesicles and that anionic

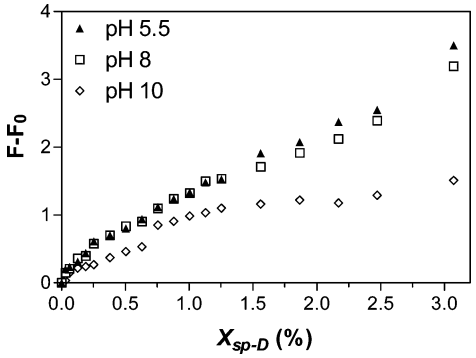


**Figure 14.** Increase in fluorescence intensity of pyrene monomer as a function of sp-D mole fraction at pH 10 (◇), pH 8 (□), and pH 5.5 (▲). Vesicles are a mixture of pyPG (1.67 $\mu$M) and POPG (213.33 $\mu$M) in 10 mM phosphate buffer. Excitation 346 nm, emission 395 nm.

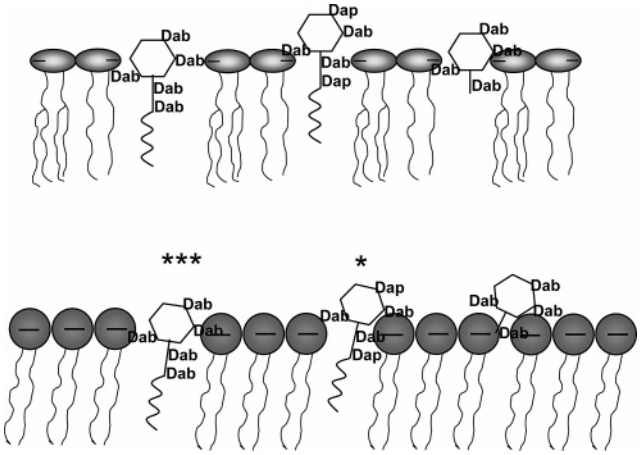


**Figure 15.** Cartoon schematic of possible interactions of the peptides with bacterial membranes. (Top) Lipopolysaccharide as OM model; (bottom) anionic phospholipid as IM model. Peptides represent (from left to right) PxB or sp-B; sp-D; and PxB-np. Active forms are marked with asterisks (see text for details).

phospholipids such as PG are exchanged between the vesicles in contact without lysis or leakage of aqueous contents.[31] Exchange is selective for monoanionic phospholipids such as PG, whereas dianionic PA is excluded[32] (data partially included in Figure 13). This biophysical phenomenon has been proposed as the mechanism of action of PxB on Gram-negative bacteria, by formation of contacts between the two phospholipid interfaces surrounding the periplasmic space of Gram-negative microorganisms.[14−16] More recently, we have shown that synthetic analogues sp-B and sp-C are able to form vesicle−vesicle contacts.[21] Resonance energy transfer experiments with fluorescently labeled derivatives of sp-B indicate that the membrane contacts are formed by peptide dimers.[22] Additional results in this paper show that sp-C vesicle−vesicle contacts induce exchange of PG but not PA (Figure 13). Interestingly, although sp-D binds and inserts into the POPG lipid interface, its ability to induce lipid exchange is very low. This result can be explained by consideration of the proposed structure of PxB in the vesicle−vesicle contacts, obtained from NMR and molecular modeling and docking calculations.[23] PxB in contacts has two well-defined binding sites for anionic phospholipids: site A, formed with residues Dab-1, Dab-3, and Dab-5, and site B, formed with the amino groups of Dab-8 and Dab-9 and the H-bonding contributions from NH and OH of Thr-10. These two sites are spatially separated and can be occupied by two separate phosphate groups, such as two molecules of POPG. In a vesicle−vesicle contact, this conformation could facilitate lipid exchange by temporally differentiated binding of a POPG molecule. In sp-D, the two mutations introduced in positions 1 and 8 (Dap instead of Dab) directly affect the two binding sites, A and B, affecting negatively the ability of the peptide to induce vesicle−vesicle lipid exchange (Figure 13). To determine if this effect is simply due to a lower content of cationic charges in sp-D at the pH of the experiments given the p$K_a$ of ≈8.5 for this amino acid,[25] we conducted the exchange experiments at different pH values, using 10 mM phosphate buffers adjusted at the desired pH value of 10, 8, or 5.5. Results shown in Figure 14 indicate that the cationic charges are important for activity, since lipid exchange is very low at pH 10, when the amino groups of both Dap are essentially deprotonated. However, experiments at pH 5.5, when most of the amino groups of Dap are protonated, show an activity that is comparable to the obtained at pH 8.0 but still significantly below that of sp-B or PxB. In conclusion, the lower capacity of sp-D to induce lipid exchange between membranes can be attributed to at least two different factors: a lower content in cationic charges and possibly a steric factor, given the shorter lateral chain of Dap compared to Dab.

## Conclusions

Data presented here emphasize the importance of the electrostatic and hydrophobic interactions in the processes of binding, insertion, and induction of lipid exchange for PxB and several analogues in the outer and inner membranes of bacteria, as shown schematically in Figure 15. Insertion into the LPS layer is achieved to different extents by all the lipopeptides assayed, including acyl chain-lacking compound PxB-np. However, insertion into the anionic phospholipid membrane and adoption of an active form of the peptides, that is, the ability to induce phospholipid exchange, is more restrictive and requires the interplay of the two hydrophobic domains of the lipopeptide (the acyl chain and the D-Phe-Leu region), and the five positive charges of Dab. In Figure 15, PxB and the analogue lipopeptide sp-B insert into the anionic phospholipid membrane and adopt the active form, indicated with the three asterisks, whereas sp-D is much less active (one asterisk in the figure), and PxB-np, which binds but does not intercalate between the phospholipid molecules, cannot induce the lipid exchange at all.

We conclude that the newly developed peptides sp-B and sp-C are good candidates for new antibiotics acting on Gram-negative bacteria by the same mechanism as PxB, because they interact with both the OM and the IM. Bacterial membranes are important for maintaining homeostasis, metabolism, and viability. Changes in membrane-specific composition, as in the case of OM−IM peptide-induced lipid exchange, will result in osmotic imbalance that leads to bacteriostasis and cell death. There is a renewed interest in the clinical use of polymyxin, due to the emergence of multidrug-resistance Gram-negative bacteria and the lack of development of new antibiotics to combat them, despite the toxicity associated with systemic use of this antibiotic. The development of PxB analogues such as those described here may generate new antibiotics with great potential for therapeutical use and with minimal potential for selection of resistance.

**Acknowledgment.** This work was supported by a grant from the Ministerio de Ciencia y Tecnología-FEDER, SAF2002-01740 (to Y.C.), BQU2003-08174 (to F.R.), and Generalitat de Catalunya, (Centre de Referència en Biotecnologia, CerBa).

## References and Notes


(1) Coates, A.; Hu, Y.; Bax, R.; Page, C. *Nat. Rev.* **2002**, *1*, 895−910.
(2) Yeaman, M. R.; Yount, N. Y. *Pharmacol. Rev.* **2003**, *55*, 27−55.
(3) Orsoya, T. *Biopolymers* **2005**, *80*, 717−735.
(4) Andreu, D.; Ribas, L. *Biopolymers* **1998**, *47*, 415−433.
(5) Brodgen, K. A. *Nat. Rev. Microbiol.* **2005**, *3*, 238−250.
(6) Zasloff, M. *Nature* **2002**, *415*, 389−395.
(7) Storm, D. R.; Rosenthal, K.; Swanson, P. E. *Annu. Rev. Biochem.* **1977**, *46*, 723−763.
(8) Falagas, M. E.; Kasiakou, S. K. *Clin. Infect. Dis.* **2005**, *40*, 1333−41.
(9) Denton, M.; Kerr, K. G. *Clin. Microbiol. Rev.* **1998**, *11*, 57−80.
(10) Ouderkirk, J. P.; Nord, J. A.; Turett, G. S.; Kislak, J. W. *Antimicrob. Agents Chemother.* **2003**, *47*, 2659−2662.
(11) Hancock, R. E. W.; Chapple, D. S. *Antimicrob. Agents Chemother.* **1999**, *43*, 1317−1323.
(12) Zhang, L.; Dhillon, P.; Yan, H.; Farmer, S.; Hancock, R. E. W. *Antimicrob. Agents Chemother.* **2000**, *44*, 3317−3321.
(13) Wu, M.; Maier, E.; Benz, R.; Hancock, R. E. W. *Biochemistry* **1999**, *38*, 7235−7242.
(14) Oh, J. T.; Van Dyk, T. K.; Cajal, Y.; Dhurjati, P. S.; Sasser, M.; Jain, M. K. *Biochem. Biophys. Res. Commun.* **1998**, *246*, 619−623.
(15) Oh, J. T.; Cajal, Y.; Skowronska, E. M.; Belkin, S.; Chen, J.; Van Dyk, T. K.; Sasser, M.; Jain, M. K. *Biochim. Biophys. Acta* **2000**, *1463*, 43−54.
(16) Liechty, A.; Chen, J.; Jain, M. K. *Biochim. Biophys. Acta* **2000**, *1463*, 55−64.
(17) Steinberg, D. A.; Hurst, M. A.; Fujii, C. A.; Kung, A. H. C.; Ho, J. F.; Cheng, F-C.; Loury, D. J.; Fides, J. C. *Antimicrob. Agents Chemother.* **1997**, *41*, 1738−1742.
(18) Tsubery, H.; Yaakov, H.; Cohen, S.; Giterman, T.; Matiyahou, A.; Fridkin, M.; Ofek, I. *Antimicrob. Agents Chemother.* **2005**, *49*, 3122−3128.
(19) Linden, P. K.; Kusne, S.; Coley, K.; Fontes, P.; Kramer, D. J.; Paterson, D. *Clin. Infect. Dis.* **2003**, *37*, 154−160.
(20) Katragkou, A.; Roilides, E. *J. Clin. Microbiol.* **2005**, *43*, 4916−4917.
(21) Clausell, A.; Rabanal, F.; García-Subirats, M.; Alsina, M. A.; Cajal, Y. *Luminescence* **2005**, *20*, 117−123.
(22) Clausell, A.; Rabanal, F.; García-Subirats, M.; Alsina, M. A.; Cajal, Y. *J. Phys. Chem. B* **2006**, *110*, 4465−4471.
(23) Bruch, M.; Cajal, Y.; Koh, J. T.; Jain, M. K. *J. Am. Chem. Soc.* **1999**, *121*, 11993−12004.
(24) Tsubery, H.; Ofek, I.; Cohen, S.; Einenstein, M.; Fridkin, M. *Mol. Pharmacol.* **2002**, *62*, 1036−1042.
(25) Farrera-Sinfreu, J.; Royo, M.; Albericio, F. *Tetrahedron Lett.* **2002**, *43*, 7813−7815.
(26) Vaara, M.; Vaara, T. *Nature* **1983**, *9*, 303−304.
(27) Rabanal, F.; Tusell, J. M.; Sastre, L.; et al. *J. Pept. Sci.* **2002**, *8*, 578−588.
(28) Maget-Dana, R. *Biochim. Biophys. Acta* **1999**, *1462*, 109−140.
(29) Davies, J. T.; Rideal, E. K. *Interfacial Phenomena*; Academic Press: New York, 1963.
(30) Hönig, D.; Möbius, D. *J. Phys. Chem.* **1991**, *95*, 4590−4592.
(31) Cajal, Y.; Rogers, J.; Berg, O. G.; Jain, M. K. *Biochemistry* **1996**, *35*, 299−308.
(32) Cajal, Y.; Ghanta, J.; Easwaran, K.; Surolia, A.; Jain, M. K. *Biochemistry* **1996**, *35*, 5684−5695.
(33) Adamson, A. W. *Physical Chemistry of Surfaces*, 3rd ed.; J. Wiley & Sons; New York, 1976; p 138.
(34) Birdi, K. S. *Lipid and Polymer Monolayers at Liquid Interfaces*; Plenum Press: New York, 1989; p 43.
(35) Miñones Jr., J.; Rodríguez-Patino, J. M.; Conde, O.; Carrera, C.; Seoane, R.; *Colloids Surf., A* **2002**, *203*, 273−286.
(36) Clausell, A.; Busquets, M. A., Pujol M., Alsina, M. A.; Cajal, Y. *Biopolymers* **2004**, *75*, 480−490.
(37) Brandenburg, K.; David, A.; Howe, J.; Koch, M. H.; Andrä, J.; Garidel, P. *Biophys. J.* **2005**, *88*, 1845−1858.
(38) Roes, S.; Seydel, U.; Gutsmann, T. *Langmuir* **2005**, *21*, 6970−6978.
(39) Gidalevitz, D.; Ishitsuka, Y.; Muresan, A. S.; Konovalov, O.; Waring, A. J.; Lehrer, R. I.; Lee, K. Y. C. *Proc. Natl. Acad. Sci. U.S.A.* **2003**, *100*, 6302−6307.
(40) Hancock, R. E. W. *Lancet* **1997**, *349*, 418−422.
(41) Xiong, Y. Q.; Mukhopadhyay, K.; Yeaman, M. R.; Adler-Moore, J.; Bayer, A. S. *Antimicrob. Agents Chemother.* **2005**, *49*, 3114−3121.
(42) Clausell, A.; Pujol, M.; Alsina, M. A.; Cajal, Y. *Talanta* **2003**, *60*, 225−234.